Origin of Pinning Disorder in Magnetic-Field-Induced Wigner Solids

Matthew L. Freeman,[1] P. T. Madathil,[2] L. N. Pfeiffer,[2] K. W. Baldwin,[2] Y. J. Chung,[2]
R. Winkler,[3] M. Shayegan,[2] and L. W. Engel[1]

[1]National High Magnetic Field Laboratory, Florida State University, Tallahassee, Florida 32310, USA
[2]Department of Electrical and Computer Engineering, Princeton University, Princeton, New Jersey 08544, USA
[3]Northern Illinois University, DeKalb, Illinois 60115, USA

At low Landau level filling factors (ν), Wigner solid phases of two-dimensional electron systems in GaAs are pinned by disorder and exhibit a pinning mode, whose frequency is a measure of the disorder that pins the Wigner solid. Despite numerous studies spanning the past three decades, the origin of the disorder that causes the pinning and determines the pinning mode frequency remains unknown. Here, we present a study of the pinning mode resonance in the low-ν Wigner solid phases of a series of ultralow-disorder GaAs quantum wells which are similar except for their varying well widths d. The pinning mode frequencies f_p decrease strongly as d increases, with the widest well exhibiting f_p as low as $\simeq 35$ MHz. The amount of reduction of f_p with increasing d can be explained remarkably well by tails of the wave function impinging into the alloy-disordered $Al_xGa_{1-x}As$ barriers that contain the electrons. However, it is imperative that the model for the confinement and wave function includes the Coulomb repulsion in the growth direction between the electrons as they occupy the quantum well.

When the Coulomb energy of a system of electrons dominates the kinetic energy, and disorder is sufficiently small, minimization of the Coulomb energy drives the formation of a Wigner solid (WS) [1], which is invariably pinned by interaction with the host system. Because of pinning by disorder, unlike the essentially uniform pinning of WS in some moiré systems [2,3], a finite correlation length of crystalline order is produced. The pinning makes the WS an insulator and also causes the spectrum of a WS to exhibit a pinning mode, a small, collective oscillation of electrons of the solid about their pinned positions. The frequency of the pinning mode is a measure of the strength of the pinning disorder. In this Letter, we utilize the pinning mode to identify the disorder pinning a WS in state-of-the-art, ultralow-disorder GaAs quantum wells [4,5] in high magnetic fields.

There is a great deal of evidence for the existence of WS in low-disorder, GaAs-hosted two-dimensional electron systems (2DESs) at high magnetic fields, which effectively freeze out the kinetic energy [6–10]. These include pinning-mode studies [11–23], $I - V$ curves [24], higher-temperature transport [25], and photoluminescence [26–28]. Most recently, evidence for the WS has also come from studies of the tunneling density of states [29], from the geometric resonance of nearby mobile carriers in a composite fermion metal by a WS in a nearby plane [30], and from NMR relaxation [31]. In low-disorder GaAs 2DESs, a WS is expected in high magnetic fields, starting near the fractional quantum Hall effect (FQHE) at Landau level filling

($\nu = 1/5$). Theoretical work [32,33] has characterized the high magnetic field WS to be composed of composite fermions [34], which can be thought of as electrons bound to an even number of flux quanta. The present study of WS pinning disorder then has relevance to the disorder that produces vanishing diagonal conductivity in FQHE states, in which composite fermions are localized, either as single particles or as a pinned solid [21]. A more detailed understanding of disorder effects on carriers in high magnetic field may also be of value to the development of quantum computation schemes utilizing FQHE quasiparticles [35].

Here, we present a study of four GaAs quantum well (QW) samples, grown by molecular beam epitaxy to be similar to each other except for their well thickness d. The samples are grown according the state of the art described in Ref. [4]. The QWs have $d = 30$, 40, 50, and 70 nm and, respectively, mobilities 10, 17, 16, and 26×10^6 cm^2/V s and carrier densities of $n = 4.5$, 4.5, 4.2, and 4.7×10^{10} cm^{-2}. While mobilities depend on n, the overall trend is of mobility increasing with d. According to the calculations in Ref. [5], with realistic estimates of the interfacial asperity characteristics, interface roughness disorder reduces the mobility for the narrower wafers. Flanking the QWs on each side are 280-nm-thick barriers of $Al_{0.12}Ga_{0.88}As$. In all four samples, only the lowest QW electric subband is populated. The QW thicknesses and carrier densities of our samples are not compatible with a low ν bilayer (two-component) WS [36–38].
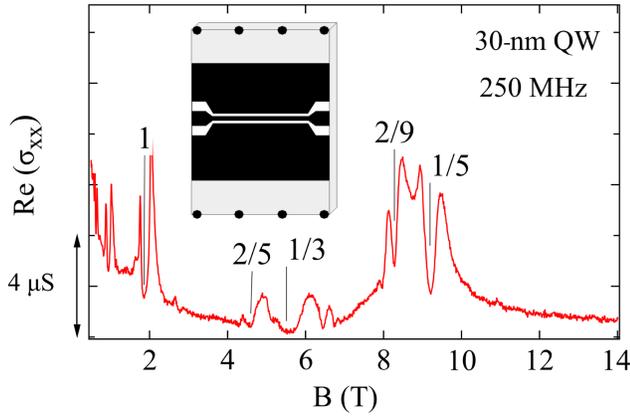
FIG. 1. Real diagonal conductivity $\mathrm{Re}(\sigma_{xx})$ vs magnetic field B for the 30-nm QW. Inset: schematic of measurement setup, with the metal film of coplanar waveguide shown as black.

We find a strong decrease in the pinning mode frequency f_p on increasing d. The measured f_p decreases by nearly an order of magnitude as d increases from 30 to 70 nm. The 70-nm-wide QW has an extremely low $f_p \simeq 35$ MHz, indicating the extremely low disorder of the sample. f_p vs d can be fit very well using a model of alloy disorder arising from penetration of the tails of the wave functions into the $Al_xGa_{1-x}As$ barriers that flank the well. To explain the data, the model must use a Poisson-Schrödinger approach that self-consistently incorporates the effect of the populated well on the charge distribution along the growth direction.

To measure the radio-frequency (rf) conductivity, we used coplanar waveguide (CPW) transmission lines patterned onto the top surfaces of the samples as shown schematically in the inset in Fig. 1. The CPW couples capacitively to the 2DES, about 900 nm below. The driven center conductor of the CPW was 75 μm wide and was separated from the grounded side planes by 50-μm-wide slots. The transmission coefficients were measured with a room-temperature network analyzer. We calculated the 2DES conductivity σ_{xx} from a distributed model of the coupled system of the CPW and 2DES. The model, described in Ref. [19], was suggested originally in Ref. [39] and takes the 2DES to be in the small-wave-vector limit. The model corrects for the tendency of the rf field in the 2DES to spread out from the region under the CPW slots near the resonance condition, particularly at low frequencies. Pinning-mode frequencies, from which the conclusions of this study are drawn, are essentially the same whether assessed from the raw transmission coefficient spectra or from the $\mathrm{Re}(\sigma_{xx})$ data shown below. The measurements were carried out in the low-power limit, in which the measured conductivity is not sensitive to the excitation power, with the 2DES at $\simeq 35$ mK, estimated from the dependence of the resonance on cryostat temperature.

The experimentally deduced 2DES conductivity $\mathrm{Re}(\sigma_{xx})$ vs magnetic field B is shown in Fig. 1 for the 30-nm QW, at a frequency of 250 MHz. Minima in $\mathrm{Re}(\sigma_{xx})$ due to FQHEs are clearly visible. The $\mathrm{Re}(\sigma_{xx})$ behavior between the 2/9 and 1/5 FQHE minima is an effect of the varying proximity of the pinning resonance frequency to the measurement frequency in that ν range. The apparent increase of $\mathrm{Re}(\sigma_{xx})$ as B goes below 4 T comes from rf parallel conduction in the sample, which freezes out as B increases.

Figure 2 shows color-scale $\mathrm{Re}(\sigma_{xx})$ spectra taken at many fillings, $0.14 < \nu < 0.22$, for the four QWs. For $\nu \lesssim 0.19$, all the QWs develop a striking, sharp resonance whose frequency f_p depends strongly on the QW thickness. Low f_p, observed particularly for the 70-nm QW, signifies a long correlation length of crystalline order. For the 70-nm QW, the number of electrons per (Larkin) domain can be estimated [39,40], as $2\pi\mu_c/eBf_p \simeq 1000$, using the classical WS shear modulus [41], $\mu_c = 0.245 e^2 n^{3/2}/4\pi\epsilon_0\epsilon$. Consistent with the interpretation of the resonance as a pinning mode, the resonance is absent in the range of the 1/5 FQHE, which is clearly visible as a low-conductivity band that appears as dark blue. As 1/5 is approached from either the higher or lower ν side, the resonance frequency f_p is reduced sharply as the resonance fades away [42]. For ν above the 1/5 FQHE, in the reentrant range [43] of the WS, up to $\nu = 0.22$, a resonance is also present, although much weaker and broader. The 40-nm QW data show a weak but sharp secondary resonance at higher frequency than that of the main peak, although such a resonance is absent in the spectra of the other samples. While likely related to the main peak, this secondary peak does not appear to be a harmonic.

The central result of this work is the pronounced decrease of f_p with increasing QW thickness. Though f_p is determined by the shear modulus (μ) of the WS as well as by the pinning disorder [39,40,44], we rule out the shear modulus effect as an explanation for the observed tenfold decrease of f_p as d is increased. μ is expected to decrease as d increases, because in a thicker well the electron-electron interaction is softer at short range. However, in the context of weak pinning [39,40,44] a softer WS results in a *larger* f_p. The inverse relationship of f_p and μ follows from the tendency of carriers, when the WS is softer, to be more closely associated with disorder potential minima and, hence, to experience larger restoring force upon displacement.

The densities n of our QWs are not identical, and n can affect f_p, because μ increases with n. For well-developed resonances in the ν ranges shown here, the expected relation is $f_p \propto n^{-3/2}$. This relationship is predicted in theory [39,40,44] and is also borne out by studies of f_p vs n [15]. To capture the trends solely due to changing d in our f_p vs d data, we multiply the measured f_p by a near-unity factor $\alpha = (n/4.5 \times 10^{10} \mathrm{\ cm}^{-2})^{3/2}$ to correct all the frequencies to their equivalents for $n = 4.5 \times 10^{10} \mathrm{\ cm}^{-2}$.
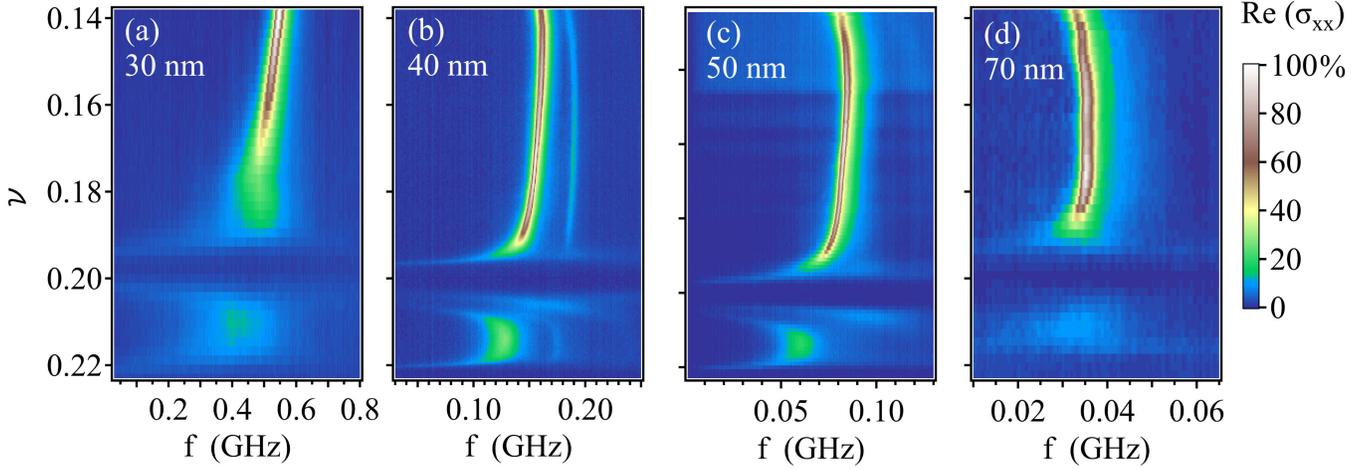
FIG. 2. Color-scale plots of real diagonal conductivity $\mathrm{Re}(\sigma_{xx})$, on frequency-filling factor (f-ν) axes, for the four QWs, marked with well widths d. The graphs are shown with larger ν at the bottom, so magnetic field B increases going upward. The color scale is in percentages of full scales, which are 50, 210, 120, and 100 μS, respectively, for (a)–(d). For the 70-nm QW of (d) only, $\mathrm{Re}(\sigma_{xx})$ is multiplied by a factor of 5 for $\nu > 0.20$, to enhance visibility in that range, which has small $\mathrm{Re}(\sigma_{xx})$.

We emphasize that the corrections are small: For $d = 30$-, 40-, 50-, and 70-nm QWs, respectively, $\alpha = 1.0, 1.0, 0.90$, and 1.07. It is clear that the variation of n from sample to sample cannot explain the large variation of f_p with d.

Figure 3 shows αf_p at $\nu = 0.15$ vs d. The graph is plotted in log-log format to account for the wide range of
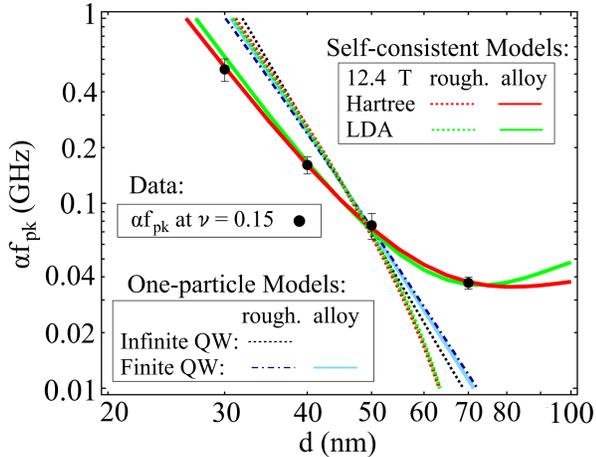
FIG. 3. Density-corrected resonance frequency αf_p (see the text) vs QW width d. Measured αf_p for the four QWs at $\nu = 0.15$ are shown as black dots. For $d = 30$, 40, 50, and 70 nm, respectively, $\alpha = 1.0, 1.0, 0.90$, and 1.07. Curves for the models discussed in the text are as shown in the legend. The one-particle infinite QW (interface roughness) and finite QW (roughness and alloy) curves are multiplied by scale factors to intercept $(d, \alpha f_p) = (45.3 \text{ nm}, 0.125 \text{ GHz})$, the centroid of the measured αf_p data points on the log-log plot. The curves marked "alloy" are the calculated P_B^2, and all "roughness" curves are the calculated $(\partial E_s / \partial d)^2$; see the text for details. The P_B^2 curves generated for the Hartree and LDA self-consistent calculations are scaled to least-squares fit the αf_p data. The fits are done on the logged αf_p data.

f_p as d is varied. The change of f_p with ν where the resonance is well developed ($0.14 \leq \nu \leq 0.19$) is shown as the error bars on the figure. The other curves in Fig. 3 show different model calculations for f_p vs d and are discussed below.

In the remainder of this Letter, we consider different sources of disorder in our samples and show how the variation of αf_p with d points to the origin of the disorder that pins the WS. The types of disorder affecting the 2DES in QWs are well known: (i) charged impurities (usually C) which are dispersed through the growth and which limit [5] the possible mobilities at zero magnetic field for dilute samples with very thick spacer layers; (ii) smooth disorder, stemming from the granularity of the remote donors grown into the sample, on a long length scale given by the spacing of the donors; (iii) interface roughness at the edges of the QW; and, finally, (iv) alloy disorder [20], from penetration of the tails of the wave functions into the $Al_x Ga_{1-x} As$ barriers, whose Al is randomly distributed. The dispersed impurities (i) would not be expected to produce the observed decreasing f_p with d. Reference [5] shows that the effect of this disorder on mobility is independent of d.

The remote ionized donors (ii) are about the same distance away from the WS for all the QWs and also would not be expected to produce the strong thickness dependence. This leaves interface roughness or alloy scattering in the barriers as candidates to explain the data.

To identify the pinning disorder, we make use of an *effective* disorder potential $V(\mathbf{r})$ to estimate the pinning energy. The effective potential takes into account the probability that the electron wave function in the WS will couple to a source of pinning disorder. In weak-pinning theory [39,40], f_p goes as a correlation function of this effective potential, $\langle V(0)V(\mathbf{r}) \rangle = V_0^2 f(r)$, where $f(r)$ is normalized to unity and decays with length much shorter

than the WS lattice constant, so $f_p \propto V_0^2$ for a given type of disorder. We model $f_p(d)$ by considering the dependence of V_0^2 on d to within a constant of proportionality, which we treat as an adjustable parameter.

Interface roughness disorder has been modeled based on the spatial fluctuations of the QW subband energy [45–47]. In this picture, asperities in the interface locally alter the well thickness and, hence, the subband energy. For an infinitely deep QW, the subband energy E_s goes as d^{-2}, and a fluctuation in d of $\xi \ll d$ produces a change in E_s of $\sim -\xi d^{-3}$. The interface roughness fluctuation size ξ should be the same for all the samples, because they were grown in the same system and under similar conditions. So in considering the sample series and taking the fluctuation in subband energy to be V_0, we find $V_0^2 \propto (\partial E_s/\partial d)^2 \propto d^{-6}$. We also obtained E_s and $(\partial E_s/\partial d)^2$ from a simple model of a finite square well, whose depth is the conduction band discontinuity, 0.095 eV [48], for the $Al_{0.12}Ga_{0.88}As$ barriers closest to the QW, and effective mass of $0.067m_0$, both inside and outside the QW, where m_0 is the free-electron mass. The $(\partial E_s/\partial d)^2$ curves for the infinite and finite square wells are shown in Fig. 3 as a dotted gray line and a dashed-dotted blue line, respectively. For comparison with the data, the curves are multiplied by prefactors to intersect the centroid of the data on the log-log plot. The slopes of the two curves are similar and are both clearly too large compared to the data.

For effective alloy disorder from the evanescent penetration of the WS charge density into the barriers, V_0 is proportional to the probability P_B that a carrier is within the barriers, so f_p is modeled to be proportional to P_B^2. In the simple, finite square QW model in the previous paragraph, P_B is obtained by integrating the tails of the charge distribution in the barriers. The resulting P_B^2, again multiplied by a factor to intersect the centroid of the data, is shown in Fig. 3 as a solid blue curve. Clearly, this line also decreases with d more strongly than the experimental f_p data.

The simple "textbook," one-particle, square-well models neglect the effect of Coulomb repulsion between the electrons along the growth direction. This repulsion tends to push charge to the edges of a QW as it is widened [49–51]. We performed self-consistent calculations of the charge distribution and potential, using the Poisson and Schrödinger equations, at magnetic field $B = 12.4$ T, and $n = 4.5 \times 10^{10}$ cm^{-2} to match $\nu = 0.15$ as in Fig. 3. Figure 4(a) shows potential and charge distributions calculated for the 30-, 50-, and 70-nm QWs in the self-consistent Hartree approximation [52]. As d increases, the charge distributions flatten and eventually become bimodal.

We carried out the self-consistent calculations for high magnetic field, with the charge density coming from the occupied Landau level only. Because of the Landau level
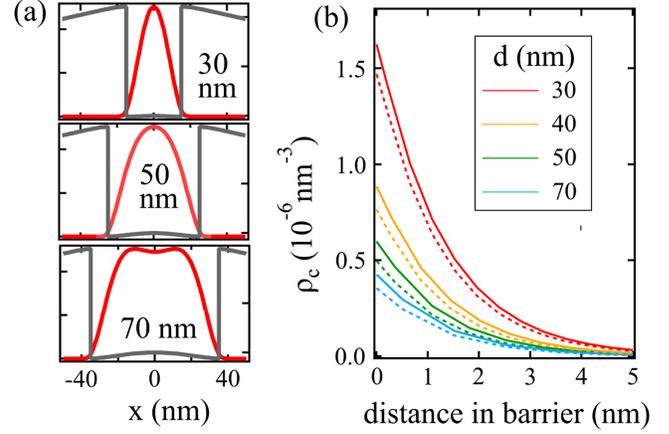
FIG. 4. (a) Normalized charge density ρ_c (red lines) and self-consistent potential V (black lines) for QWs of widths $d = 30$, 50, and 70 nm. These are from Poisson-Schrödinger, self-consistent (Hartree) calculations for $B = 12.4$ T. (b) Hartree (solid line) and LDA (dashed line) calculated charge distribution tails within the barriers, for the four QWs. The edge of the barrier is the origin of the horizontal axis.

degeneracy, the second electric subband, occupied for $d > 70$ nm at $B = 0$, is not occupied in high field. We evaluated the wave functions of the Landau levels via an 8×8 multiband Hamiltonian [52]. Besides the self-consistent Hartree approximation, we also used spin density-functional theory in the local-density approximation (LDA) based on the spin-dependent exchange-correlation potential parametrized in Ref. [53].

Estimates of the effect of interface roughness in the context of the self-consistent calculations come from taking $f_p \propto (\partial E_s/\partial d)^2$, with $E_s(d)$ (measured from the well center) coming from the self-consistent calculations. The Hartree and LDA calculations give the red and green dotted curves in Fig. 3, respectively. The curves are again multiplied by scale factors to intercept the centroid of the measured data. The curves are nearly identical and decrease much more strongly than the experimental data.

In Fig. 3, the red and green solid curves show P_B^2 vs d obtained from the Hartree and LDA calculations, respectively, multiplied by scale factor parameters to least-squares fit the density-adjusted experimental data αf_p. The fits are remarkably good. P_B^2 is proportional to the contribution of alloy disorder to f_p, so the good fits suggest that the charge density in the barriers is indeed the origin of the pinning disorder and that the self-consistent modeling of the populated well is required to reasonably estimate the P_B associated with the charge density in the barriers. In comparison to the one-particle square-well models, the self-consistent models lessen the effect of the widening well, because the pushing outward of the charge distributions from Coulomb repulsion preserves more charge density in the barriers as the well gets wider. In the theoretical curves, this effect continues at larger d, so that the curves increase for $d > 70$ nm.

The self-consistent models are only approximations, because they take the charge as uniform sheets in the 2D plane, which is not the case in a WS. For our samples with $n \simeq 4.5 \times 10^{10}$ cm^{-2}, the effective in-plane size of an electron is the magnetic length $l_B \simeq 7$ nm at $\nu = 0.15$, while the WS lattice constant $a = 2^{1/2} \times 3^{-1/4} n^{-1/2} \simeq 50$ nm. In between WS lattice sites, because of the smaller charge density, the penetration of charge into the barriers will be somewhat less than the model estimates. Likewise, more penetration than predicted will occur at lattice sites. These effects would not vary much with d, explaining the strikingly good fits we see.

In summary, we have studied the pinning mode of the magnetic-field-induced WS in a series of ultralow-disorder GaAs QW samples, of varying thickness. An extremely low f_p down to 35 MHz is found in the 70-nm QW. We identify the disorder responsible for the WS pinning as Al alloy disorder in the QW barriers. For this disorder, the decreasing curve of f_p vs well thickness is quantitatively explained by the reduction of charge density in the barriers for thicker wells, if this reduction is self-consistently evaluated to account for the QW population.

[1] E. Wigner, On the interaction of electrons in metals, Phys. Rev. **46**, 1002 (1934).

[2] M. Shayegan, Wigner crystals in flat band 2D electron systems, Nat. Rev. Phys. **4**, 212 (2022).

[3] B. Padhi, R. Chitra, and P. W. Phillips, Generalized Wigner crystallization in moiré materials, Phys. Rev. B **103**, 125146 (2021).

[4] Y. J. Chung, K. A. Villegas Rosales, K. W. Baldwin, P. T. Madathil, K. W. West, M. Shayegan, and L. N. Pfeiffer, Ultra-high-quality two-dimensional electron systems, Nat. Mater. **20**, 632 (2021).

[5] Y. J. Chung, A. Gupta, K. W. Baldwin, K. W. West, M. Shayegan, and L. N. Pfeiffer, Understanding limits to mobility in ultrahigh-mobility GaAs two-dimensional electron systems: 100 million cm^2/V s and beyond, Phys. Rev. B **106**, 075134 (2022).

[6] Y. E. Lozovik and V. Yudson, Crystallisation of a two dimensional electron gas in magnetic field, JETP Lett. **22**, 11 (1975).

[7] P. K. Lam and S. M. Girvin, Liquid-solid transition and the fractional quantum-Hall effect, Phys. Rev. B **30**, 473 (1984).

[8] D. Levesque, J. J. Weis, and A. H. MacDonald, Crystallization of the incompressible quantum-fluid state of a two-dimensional electron gas in a strong magnetic field, Phys. Rev. B **30**, 1056 (1984).

[9] K. Yang, F. D. M. Haldane, and E. H. Rezayi, Wigner crystals in the lowest Landau level at low-filling factors, Phys. Rev. B **64**, 081301(R) (2001).

[10] M. Shayegan, in *Perspectives in quantum Hall effects*, edited by S. das Sarma and A. Pinczuk (Wiley-Interscience, New York, 1997), p. 343.

[11] E. Y. Andrei, G. Deville, D. C. Glattli, F. I. B. Williams, E. Paris, and B. Etienne, Observation of a magnetically induced Wigner solid, Phys. Rev. Lett. **60**, 2765 (1988).

[12] F. I. B. Williams, P. A. Wright, R. G. Clark, E. Y. Andrei, G. Deville, D. C. Glattli, O. Probst, B. Etienne, C. Dorin, C. T. Foxon, and J. J. Harris, Conduction threshold and pinning frequency of magnetically induced Wigner solid, Phys. Rev. Lett. **66**, 3285 (1991).

[13] M. A. Paalanen, R. L. Willett, P. B. Littlewood, R. R. Ruel, K. W. West, L. N. Pfeiffer, and D. J. Bishop, rf conductivity of a two-dimensional electron system at small Landau-level filling factors, Phys. Rev. B **45**, 11342 (1992).

[14] L. W. Engel, C. C. Li, D. Shahar, D. C. Tsui, and M. Shayegan, Microwave resonances in low-filling insulating phase of two-dimensional electron system, Solid State Commun. **104**, 167 (1997).

[15] C.-C. Li, J. Yoon, L. W. Engel, D. Shahar, D. C. Tsui, and M. Shayegan, Microwave resonance and weak pinning in two-dimensional hole systems at high magnetic fields, Phys. Rev. B **61**, 10905 (2000).

[16] P. D. Ye, L. W. Engel, D. C. Tsui, R. M. Lewis, L. N. Pfeiffer, and K. West, Correlation lengths of the Wigner-crystal order in a two-dimensional electron system at high magnetic fields, Phys. Rev. Lett. **89**, 176802 (2002).

[17] Y. P. Chen, R. M. Lewis, L. W. Engel, D. C. Tsui, P. D. Ye, Z. H. Wang, L. N. Pfeiffer, and K. W. West, Evidence for two different solid phases of two-dimensional electrons in high magnetic fields, Phys. Rev. Lett. **93**, 206805 (2004).

[18] Y. P. Chen, G. Sambandamurthy, Z. H. Wang, R. M. Lewis, L. W. Engel, D. C. Tsui, P. D. Ye, L. N. Pfeiffer, and K. W. West, Melting of a 2D quantum electron solid in high magnetic field, Nat. Phys. **2**, 452 (2006).

[19] Z. Wang, Y. P. Chen, H. Zhu, L. W. Engel, D. C. Tsui, E. Tutuc, and M. Shayegan, Unequal layer densities in bilayer Wigner crystal at high magnetic fields, Phys. Rev. B **85**, 195408 (2012).

[20] B.-H. Moon, L. W. Engel, D. C. Tsui, L. N. Pfeiffer, and K. W. West, Pinning modes of high-magnetic-field Wigner solids with controlled alloy disorder, Phys. Rev. B **89**, 075310 (2014).

[21] H. Zhu, Y. P. Chen, P. Jiang, L. W. Engel, D. C. Tsui, L. N. Pfeiffer, and K. W. West, Observation of a pinning mode in a Wigner solid with 1/3 fractional quantum Hall excitations, Phys. Rev. Lett. **105**, 126803 (2010).

[22] A. T. Hatke, H. Deng, Y. Liu, L. W. Engel, L. N. Pfeiffer, K. W. West, K. W. Baldwin, and M. Shayegan, Wigner solid pinning modes tuned by fractional quantum Hall states of a nearby layer, Sci. Adv. **5,** 2848 (2019).

[23] L. Zhao, W. Lin, Y. J. Chung, A. Gupta, K. W. Baldwin, L. N. Pfeiffer, and Y. Liu, Dynamic response of Wigner crystals, Phys. Rev. Lett. **130,** 246401 (2023).

[24] V. J. Goldman, M. Santos, M. Shayegan, and J. E. Cunningham, Evidence for two-dimentional quantum Wigner crystal, Phys. Rev. Lett. **65,** 2189 (1990).

[25] W. Pan, H. L. Stormer, D. C. Tsui, L. N. Pfeiffer, K. W. Baldwin, and K. W. West, Transition from an electron solid to the sequence of fractional quantum Hall states at very low Landau level filling factor, Phys. Rev. Lett. **88,** 176802 (2002).

[26] E. M. Goldys, S. A. Brown, R. B. Dunford, A. G. Davies, R. Newbury, R. G. Clark, P. E. Simmonds, J. J. Harris, and C. T. Foxon, Magneto-optical probe of two-dimensional electron liquid and solid phases, Phys. Rev. B **46,** 7957 (1992).

[27] H. Buhmann, W. Joss, K. von Klitzing, I. V. Kukushkin, A. S. Plaut, G. Martinez, K. Ploog, and V. B. Timofeev, Novel magneto-optical behavior in the Wigner-solid regime, Phys. Rev. Lett. **66,** 926 (1991).

[28] I. V. Kukushkin, V. I. Falko, R. J. Haug, K. von Klitzing, K. Eberl, and K. Totemayer, Evidence of the triangular lattice of crystallized electrons from time resolved luminescence, Phys. Rev. Lett. **72,** 3594 (1994).

[29] J. Jang, B. M. Hunt, L. N. Pfeiffer, K. W. West, and R. C. Ashoori, Sharp tunnelling resonance from the vibrations of an electronic Wigner crystal, Nat. Phys. **13,** 340 (2016).

[30] H. Deng, Y. Liu, I. Jo, L. N. Pfeiffer, K. W. West, K. W. Baldwin, and M. Shayegan, Commensurability oscillations of composite fermions induced by the periodic potential of a Wigner crystal, Phys. Rev. Lett. **117,** 096601 (2016).

[31] L. Tiemann, T. D. Rhone, N. Shibata, and K. Muraki, NMR profiling of quantum electron solids in high magnetic fields, Nat. Phys. **10,** 648 (2014).

[32] J.-W. Rhim, J. K. Jain, and K. Park, Analytical theory of strongly correlated Wigner crystals in the lowest Landau level, Phys. Rev. B **92,** 121103(R) (2015).

[33] A. C. Archer and J. K. Jain, Phase diagram of the two-component fractional quantum Hall effect, Phys. Rev. Lett. **110,** 246801 (2013).

[34] J. K. Jain, *Composite Fermions* (Cambridge University Press, Cambridge, England, 2007).

[35] C. Nayak, S. H. Simon, A. Stern, M. Freedman, and S. Das Sarma, Non-Abelian anyons and topological quantum computation, Rev. Mod. Phys. **80,** 1083 (2008).

[36] S. Narasimhan and T.-L. Ho, Wigner-crystal phases in bilayer quantum Hall systems, Phys. Rev. B **52,** 12291 (1995).

[37] H. C. Manoharan, Y. W. Suen, M. B. Santos, and M. Shayegan, Evidence for a bilayer quantum Wigner solid, Phys. Rev. Lett. **77,** 1813 (1996).

[38] A. T. Hatke, Y. Liu, L. W. Engel, M. Shayegan, L. N. Pfeiffer, K. W. West, and K. W. Baldwin, Microwave spectroscopy of the low-filling-factor bilayer electron solid in a wide quantum well, Nat. Commun. **6,** 7071 (2015).

[39] M. M. Fogler and D. A. Huse, Dynamical response of a pinned two-dimensional Wigner crystal, Phys. Rev. B **62,** 7553 (2000).

[40] R. Chitra, T. Giamarchi, and P. Le Doussal, Pinned Wigner crystals, Phys. Rev. B **65,** 035312 (2001).

[41] L. Bonsall and A. A. Maradudin, Some static and dynamical properties of a two-dimensional Wigner crystal, Phys. Rev. B **15,** 1959 (1977).

[42] L. V. Delacrétaz, B. Goutéraux, S. A. Hartnoll, and A. Karlsson, Theory of collective magnetophonon resonance and melting of a field-induced Wigner solid, Phys. Rev. B **100,** 085140 (2019).

[43] H. W. Jiang, R. L. Willett, H. L. Stormer, D. C. Tsui, L. N. Pfeiffer, and K. W. West, Quantum liquid versus electron solid around $\nu = 1/5$ Landau-level filling, Phys. Rev. Lett. **65,** 633 (1990).

[44] H. A. Fertig, Electromagnetic response of a pinned Wigner crystal, Phys. Rev. B **59,** 2120 (1999).

[45] H. Sakaki, T. Noda, K. Hirakawa, M. Tanaka, and T. Matsusue, Interface roughness scattering in GaAs/AlAs quantum wells, Appl. Phys. Lett. **51,** 1934 (1987).

[46] D. Kamburov, K. W. Baldwin, K. W. West, M. Shayegan, and L. N. Pfeiffer, Interplay between quantum well width and interface roughness for electron transport mobility in GaAs quantum wells, Appl. Phys. Lett. **109,** 232105 (2016).

[47] D. R. Luhman, D. C. Tsui, L. N. Pfeiffer, and K. W. West, Electronic transport studies of a systematic series of GaAs/AlGaAs quantum wells, Appl. Phys. Lett. **91,** 072104 (2007).

[48] S. Adachi, GaAs, AlAs, and $Al_xGa_{1-x}As$ material parameters for use in research and device applications, J. Appl. Phys. **58,** R1 (1985).

[49] Y. W. Suen, J. Jo, M. B. Santos, L. W. Engel, S. W. Hwang, and M. Shayegan, Missing integral quantum Hall effect in a wide single quantum well, Phys. Rev. B **44,** 5947 (1991).

[50] Y. W. Suen, L. W. Engel, M. B. Santos, M. Shayegan, and D. C. Tsui, Observation of a $\nu = 1/2$ fractional quantum Hall state in a double-layer electron system, Phys. Rev. Lett. **68,** 1379 (1992).

[51] H. C. Manoharan, Y. W. Suen, M. B. Santos, and M. Shayegan, Evidence for a bilayer quantum Wigner solid, Phys. Rev. Lett. **77,** 1813 (1996).

[52] R. Winkler, *Spin-Orbit Coupling Effects in Two-Dimensional Electron and Hole Systems* (Springer, New York, 2003).

[53] J. P. Perdew and A. Zunger, Self-interaction correction to density-functional approximations for many-electron systems, Phys. Rev. B **23,** 5048 (1981).